The influence of membrane air spring cord parameters on the vertical stiffness

Xufei Wang[1], Zhiqiang Xie[2], Ningchao Zhang[3], Jinde Song[4]
[1, 2, 3]School of Mechanical Engineering, Shaanxi University of Technology, Hanzhong, China
[4]Jiangsu Zhonggui Heavy Industry Co., Ltd., Yancheng, China
[1]Corresponding author
E-mail: [1]*wxf@snut.edu.cn*, [2]*xiezhiqiang@snut.edu.cn*, [3]*zhangningchao@snut.edu.cn*, [4]*910425366@qq.com*

Received 30 November 2025; accepted 13 March 2026; published online 19 April 2026
DOI https://doi.org/10.21595/jve.2026.25874

Check for updates

Copyright © 2026 Xufei Wang, et al. This is an open access article distributed under the Creative Commons Attribution License, which permits unrestricted use, distribution, and reproduction in any medium, provided the original work is properly cited.

Abstract. The membrane air spring possesses the advantage of variable vertical stiffness. However, under limited vertical installation space, further investigation is required to analyze how variations in the rubber airbag cord parameters influence the vertical stiffness of membrane air springs. A finite element model of a specific membrane air spring was developed. Under a compression displacement of 40 mm, the effects of parameters such as the number of rubber airbag cord layers, cord spacing, cord angle, and cord cross-sectional area on vertical stiffness were examined. The results indicate that vertical stiffness decreases with an increase in cord spacing or cord angle, but increases with greater cord cross-sectional area or number of cord layers. Subsequently, the orthogonal experimental method was applied to construct an L_9 (3^4) orthogonal table, and the influence of the four cord parameters on the vertical stiffness of the membrane air spring under 40 mm compression displacement was analyzed. The findings revealed that vertical stiffness is least affected by cord angle and most affected by the number of cord layers. The variation trend of vertical stiffness was determined by fitting the optimal parameter combination. Finally, the combination of four cord parameters yielding the maximum vertical stiffness was evaluated when the compression displacement increased to 50 mm, providing a reference for air spring configuration design in confined spaces.

Keywords: membrane air spring, rubber airbag, vertical stiffness, cord parameters, orthogonal experimental method.

1. Introduction

Air springs are widely employed as crucial vibration-damping components in vehicle suspension systems and air-floating vibration isolation platforms due to their advantages, including adjustable vertical stiffness, low natural frequency, and nonlinear damping characteristics [1]. In large-load vibration isolation platforms used in high-end equipment such as carrier rockets, the installation space is often restricted. Under such limitations, the vertical stiffness of conventional air springs often fails to meet the performance requirements of large-load vibration isolation systems. Therefore, it is of practical significance to study the structural characteristics and parameter variations of rubber airbags in air springs to improve their vertical stiffness in confined spaces.

In recent years, researchers have conducted numerous studies on the vertical stiffness of air springs from the perspectives of cord parameters and other structural factors. Regarding the effect of cord parameters on vertical stiffness, Zhou, et al. [2] established a finite element model of a membrane air spring based on its nonlinear material properties, geometric configuration, and contact behavior. The results indicated that, within a certain range, cord parameters are key factors influencing the vertical stiffness characteristics of membrane air springs. Lee and Kim [3] developed a relationship between the laying angle of the cord layer and its radial position by analyzing deformation patterns under different load conditions, including vertical, lateral, and torsional loads. By comparing different layup angles, they examined how these variations affect

the vertical, lateral, and torsional stiffness of the air spring. Zhang, et al. [4] discussed the nonlinear behavior of air springs from the perspectives of capsule material properties and the geometric configuration of rubber airbags. A sensitivity analysis of bladder-type air springs revealed that the number of cord layers exerts the most significant influence on vertical stiffness. To further investigate the aging mechanism of air springs, Lu, et al. [5] analyzed the effects of aging time on the vertical static stiffness of air springs. The study demonstrated that the vertical static stiffness increases with aging time, and that the aging of both the air spring cord material and rubber material contributes to this increase.

In addition, several researchers have examined the vertical stiffness of air springs from the perspective of innovative structural designs. Yin, et al. [6] proposed an air spring-based dynamic vibration absorber and investigated its damping and vibration reduction performance. The results showed that, by properly adjusting the air pressure and the throttle opening, the air spring vibration absorber could achieve a suitable vibration absorption frequency and damping ratio, thereby obtaining a broad vibration reduction effect. Oman and Nagode [7] analyzed two types of piston structures and compared their load–deformation characteristics and fatigue life. Their findings showed that the simulated and experimental vertical dynamic stiffness results were consistent with theoretical predictions. Marini, et al. [8] studied an air spring system consisting of a primary pneumatic chamber and multiple auxiliary air storage tanks, where airflow between the chambers was controlled by an adjustable valve. This configuration allowed for regulation of the equivalent spring stiffness by altering the airflow distribution.

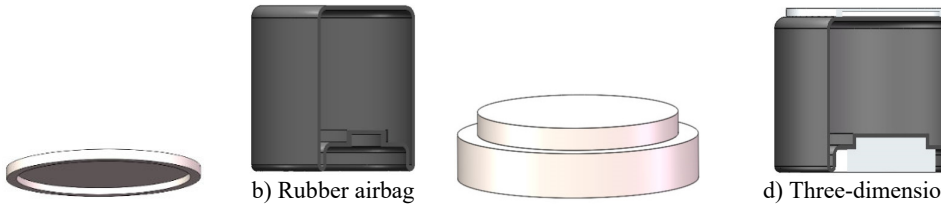
The studies conducted by these researchers can generally be divided into two categories of air spring types: bladder air springs and membrane air springs. Between these, membrane air springs exhibit smaller variations in vertical stiffness and smoother elastic characteristic curves, which make them more suitable for applications requiring stable stiffness performance.

To further analyze the influence of rubber airbag cord parameters on the vertical stiffness of membrane air springs within restricted installation spaces, parameters such as cord spacing, cord angle, cord cross-sectional area, and the number of cord layers were selected for investigation. The orthogonal experimental method was adopted to analyze the variation patterns of vertical stiffness under two different compression displacements, thereby revealing the influence laws of these four cord parameters on the vertical stiffness behavior of membrane air springs.

2. Membrane air spring structure and vertical stiffness

A specific type of membrane air spring was selected as the research object. The outer contour height of the membrane air spring is 347 mm, the radius around the rotation axis is 144 mm, and its mass is 13.214 kg. The distance between two adjacent installation holes is 158.8 mm, the maximum working pressure is 5.0 bar, and the stroke is 431.0 mm.

The membrane air spring was modeled using SolidWorks software. The upper cover plate, rubber airbag, and bottom piston were respectively modeled as shown in Figs. 1(a), (b), and (c). Fig. 1(d) presents the three-dimensional assembly drawing.



a) Upper cover plate b) Rubber airbag c) Bottom piston d) Three-dimensional assembly drawing

Fig. 1. Composition and overall structure of the membrane air spring

The nonlinearity of the vertical stiffness of the membrane air spring mainly arises from the deformation stiffness of the rubber airbag, as shown in Fig. 1(b) [9]. During compression, the

stiffness is influenced by changes in the effective area of the compressed air column and the deformation characteristics of the rubber airbag itself. The total stiffness can be expressed by Eq. (1):

$$K_t = K_1 + K_2, \tag{1}$$

where Eq. (1), K_t represents the total vertical stiffness of the membrane air spring, K_1 denotes the vertical stiffness of the compressed air, and K_2 is the deformation stiffness of the rubber airbag.

The variation of K_1, representing the vertical stiffness of the compressed air, can be divided into two stages: a linear stage and a nonlinear stage. In the linear stage, K_1 assumes that the gas inside the rubber airbag behaves as an ideal gas. When the compression displacement of the membrane air spring is small, the change in gas state within the rubber airbag is linear and can be regarded as an isothermal process. Therefore, the pressure (P) and volume (V) of the gas satisfy Boyle's Law [10]:

$$F = P_a \cdot A, \tag{2}$$
$$P_0 \cdot V_0 = P_a \cdot V_a = C, \tag{3}$$
$$V_a = V_0 - A \cdot z, \tag{4}$$

where Eq. (2), F is the load-bearing capacity of the membrane air spring, P_a is the internal pressure of the rubber airbag under compression, and A is the effective internal area of the rubber airbag. In Eq. (3), P_0 denotes the gas pressure of the rubber airbag in its initial state, V_0 is the initial volume of the rubber airbag, V_a represents the compressed volume of the rubber airbag, and C is a constant. In Eq. (4), z is the vertical displacement of the membrane air spring.

Based on Eqs. (2-4), the load-bearing capacity F of the membrane air spring can be expressed as Eq. (5):

$$F = \frac{AP_0V_0}{V_a} = \frac{AP_0V_0}{V_0 - A \cdot z}. \tag{5}$$

By differentiating F with respect to z according to Eq. (5), the vertical stiffness of the compressed air K_1 can be expressed as Eq. (6):

$$K_1 = \frac{A^2P_0V_0}{(V_0 - A \cdot z)^2}. \tag{6}$$

As the compression displacement increases further, the state of the gas within the rubber airbag gradually deviates from the linear relationship. During this nonlinear stage, the gas behavior follows a more general variable process equation [11], expressed as Eq. (7):

$$K_1 = \frac{\lambda A^2P_0V_0^{\lambda}}{(V_0 - Az)^{\lambda+1}}, \tag{7}$$

where Eq. (7), λ represents the gas process coefficient.

It follows from Eq. (7) that the vertical stiffness K_1 of the membrane air spring is related to the initial gas pressure P_0 of the rubber airbag, its initial volume V_0, the effective area A inside the airbag, and the vertical displacement z of the membrane air spring.

The deformation stiffness K_2 of the rubber airbag is composed of the stiffness K_c generated by the cord component and the stiffness K_r generated by the pure rubber component, as expressed by Eq. (8). Due to the complexity of the structure and the absence of a unified theoretical expression, it is necessary to analyze four key cord parameters-number of cord layers (t), cord spacing (m), cord angle (α), and cross-sectional area of the cord (s) – for the specific design:

$$K_2 = K_c + K_r, \tag{8}$$
$$K_c = C_{cord}\ (t, \alpha, m, s). \tag{9}$$

Since the effect of the pure rubber material on K_r is minimal and can be neglected, this study focuses on investigating the effects of the number of cord layers, cord spacing, cord angle, and cord cross-sectional area on K_c.

3. Finite element simulation of membrane air spring

3.1. Rubber material model

The rubber airbag of the membrane air spring is primarily composed of rubber material. During operation, the rubber is subjected to varying internal pressures, resulting in large elastic deformations. Therefore, the Mooney-Rivlin model was selected to simulate the nonlinear elastic behavior of the rubber. The functional expression of the Mooney-Rivlin model is given in Eq. (10):

$$U = C_{10}\ (I_1 - 3) + C_{01}\ (I_2 - 3) + C_{11}(I_1 - 3)(I_2 - 3). \tag{10}$$

where, U represents the strain potential energy of the rubber material; I_1 and I_2 are the first and second strain invariants, respectively; C_{10}, C_{01}, and C_{11} are material constants characterizing the hyperelastic behavior of rubber. Their numerical values depend on the compound formulation, operating temperature, and volumetric strain state. In practice, these constants are typically identified through nonlinear regression of uniaxial, biaxial, or inflation test data.

3.2. Structure of the rubber airbag cord layer

The cord layer plays a decisive role in determining the vertical stiffness and durability of membrane air springs [12]. To accurately describe the structural configuration and parameters of the rubber airbag cord layer, the local capsule skin shown in Fig. 1(b) was sectioned, as illustrated in Fig. 2. The local capsule skin was magnified tenfold, and the cross-section A-A perpendicular to the cord direction was selected to construct the sectional view of the cut capsule skin. Fig. 2 presents the schematic cross-sectional view for a curtain layer comprising two layers.

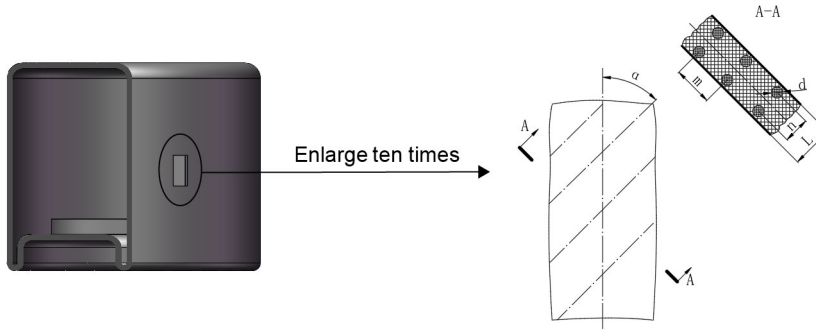


Fig. 2. Schematic diagram of the cord layer structure of the rubber airbag

In Fig. 2, α denotes the cord angle, which is the angle between the projection of a single cord's direction and the rotation center axis. d represents the diameter of a single cord's cross-section, while s is the cross-sectional area of the cord, defined as $s = \frac{\pi}{4}d^2$. m denotes the cord spacing, referring to the distance between the central axes of two adjacent cords. n represents the spacing between the axes of two adjacent cord layers, and L indicates the thickness of the rubber airbag wall of the membrane air spring.

3.3. Definition of the fluid cavity

To simulate and analyze the gas flow behavior within the rubber airbag during operation, it was necessary to define the reference point coordinates of the fluid elements and the fluid cavity. The membrane air spring model created in SolidWorks was imported into ABAQUS software, where the F3D4 fluid element was selected for the internal air cavity. The F3D4 element is a five-node pyramid element, with its apex node serving as the reference point of the fluid cavity and the four base nodes corresponding to nodes on the inner surface of the cavity. A Cartesian coordinate system was established, with the origin O (0, 0, 0) positioned at the top of the central axis of the upper cover plate. The reference point O′ of the rubber airbag's fluid cavity was defined at $(x, y, z) = (0, -10, 0)$, as shown in Fig. 3.

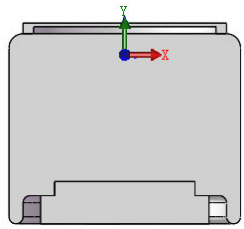


Fig. 3. Reference point of the fluid cavity



Fig. 4. Mesh model of the membrane air spring

3.4. Finite element model of the membrane air spring

In ABAQUS, the rubber airbag was meshed using tetrahedral four-node shell element S4R, while the upper cover plate and bottom piston were meshed using hexahedral eight-node R3D3 and R3D4, respectively. The average side length of the mesh elements was 3.35 mm, resulting in a total of 77,818 elements and 77,238 nodes. The generated mesh model is illustrated in Fig. 4.

Boundary conditions were then applied. Since the rubber airbag is composed mainly of rubber material, contact interactions were defined in the Interaction Module using the Constraint Manager Toolbox. Contact between the rubber airbag and the upper cover plate, as well as between the rubber airbag and the bottom piston, was set as a TIE constraint [13]. Two simulation steps were defined: inflation and loading. When the membrane air spring was at its initial height, the Predefined Field Manager Toolbox in the Load Module was used to define the internal fluid cavity pressure as 0.3 MPa. The compression direction of the base was set as the positive direction of the Y-axis in the Boundary Condition Manager Toolbox, with a specified compression displacement U_2 of 40 mm.

4. Analysis of the influence of cord layer parameters on the vertical stiffness of membrane air spring

4.1. Determination of cord layer parameters

The Section Manager Toolbox in the Property Module was used to select the cross-section of the rubber airbag. The Rebar Layers were defined according to the required cord layer parameters, and values for cord spacing (m), cord angle (α), cord cross-sectional area (s), and number of cord layers (t) were entered. Thus, the rubber airbag cord layer model was constructed. The selected cord parameter values are listed in Table 1.

Based on the cord parameters in Table 1, various combinations were established. The load and compression displacements were computed using the direct method and the Newton-Raphson method, respectively, to obtain the corresponding vertical stiffness values. The influence of each parameter combination on vertical stiffness was subsequently analyzed.

ISSN PRINT 1392-8716, ISSN ONLINE 2538-8460

Table 1. Geometric parameter values of cord

Geometric characteristics	Simulation parameters
m (mm)	3, 5, 7
α (°)	5, 10, 15
s (mm^2)	0.100, 0.166, 0.283
t (layers)	2, 4, 6

4.2. Influence of cord layer parameters on the vertical stiffness of the membrane air spring

First, the variations in the vertical stiffness of the air spring are analyzed with respect to changes in each of the four cord parameters. Subsequently, the cord layer spacing, cord angles, and cord cross-sectional area are individually varied according to the values specified in Table 1, while all of the other parameters are held constant. The corresponding calculated results for vertical stiffness are presented in Table 2.

Table 2. Calculated results for vertical stiffness

	t-m-α-s	K_1 (N·mm^{-1})
Cord layer spacing	2-3-15-0.283	51.413
	2-5-15-0.283	42.235
	2-7-15-0.283	35.525
	4-3-15-0.283	103.748
	4-5-15-0.283	88.791
	4-7-15-0.283	78.652
	6-3-15-0.283	124.443
	6-5-15-0.283	110.875
	6-7-15-0.283	101.487
Cord angles	2-3-5-0.100	47.575
	2-3-10-0.100	40.875
	2-3-15-0.100	31.532
	4-3-5-0.100	84.811
	4-3-10-0.100	80.625
	4-3-15-0.100	72.775
	6-3-5-0.100	105.375
	6-3-10-0.100	102.915
	6-3-15-0.100	95.975
Cord cross-sectional area	2-3-15-0.100	31.476
	2-3-15-0.166	41.775
	2-3-15-0.283	51.393
	4-3-15-0.100	72.775
	4-3-15-0.166	88.148
	4-3-15-0.283	103.751
	6-3-15-0.100	95.975
	6-3-15-0.166	110.275
	6-3-15-0.283	124.443

Thereafter, using the aforementioned three cord parameters as horizontal axes and vertical stiffness as the vertical axis, graphical representations were generated for air springs with 2, 4, and 6 cord layers, as illustrated in Fig. 5.

According to Table 2 and Fig. 5(a), when the number of cord layers remained constant, the vertical stiffness of the membrane air spring decreased with increasing cord spacing, indicating a negative correlation. For cord layers of 2, 4, and 6, the vertical stiffness decreased by 15.888 N/mm, 25.096 N/mm, and 22.956 N/mm, respectively, as the cord spacing increased from 3 to 7 mm. The corresponding reduction ratios were 30.9 %, 24.2 %, and 18.4 %, respectively. These results indicate that as the number of cord layers increased, the effect of larger cord spacing on reducing vertical stiffness became progressively weaker.

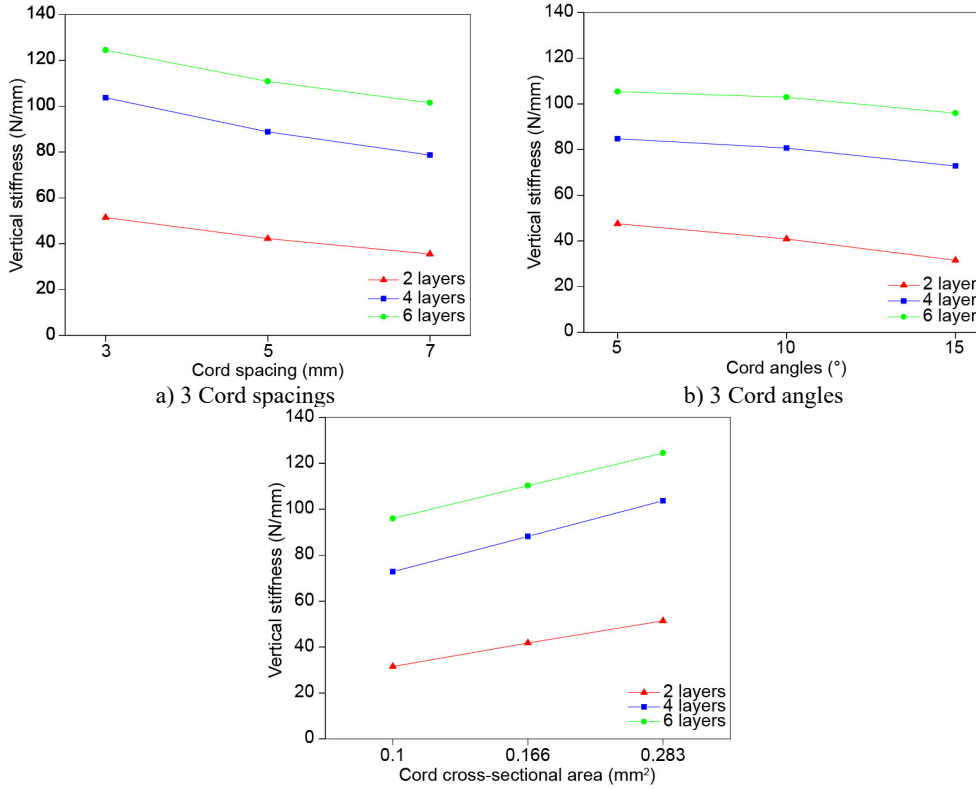


Fig. 5. Vertical stiffness characteristics of membrane air springs with different cord layer parameters

When the cord spacing remained constant, vertical stiffness increased with the number of cord layers. For cord spacings of 3, 5, and 7 mm, the increase in vertical stiffness as the number of cord layers rose from 2 to 6 was 73.030 N/mm, 68.640 N/mm, and 65.962 N/mm, respectively. The corresponding increase ratios were 142.0 %, 162.5 %, and 185.7 %, respectively. When the cord spacing was small, the number of cord layers exerted a pronounced effect on the value of vertical stiffness, but a comparatively weaker effect on its rate of change. Conversely, as cord spacing increased, the number of cord layers had a smaller effect on the stiffness value but a greater influence on its rate of change. The minimum vertical stiffness of 35.525 N/mm occurred with 2 cord layers and a spacing of 7 mm, while the maximum vertical stiffness of 124.443 N/mm was obtained with 6 cord layers and a spacing of 3 mm.

According to Table 2 and Fig. 5(b), when the number of cord layers was constant, the vertical stiffness of the membrane air spring decreased with increasing cord angle, demonstrating a negative correlation. For 2, 4, and 6 cord layers, the reductions in vertical stiffness as the cord angle increased from 5° to 15° were 16.043 N/mm, 12.036 N/mm, and 9.400 N/mm, respectively, corresponding to decrease ratios of 33.7 %, 14.2 %, and 8.9 %. These results indicate that as the number of cord layers increases, the influence of a larger cord angle on reducing vertical stiffness weakens progressively.

When the cord angle remained constant, the vertical stiffness increased with the number of cord layers. For cord angles of 5°, 10°, and 15°, as the number of cord layers increased from 2 to 6, the vertical stiffness increased by 57.800 N/mm, 62.040 N/mm, and 64.443 N/mm, respectively, corresponding to increase ratios of 121.5 %, 151.8 %, and 204.4 %. This indicates that as the number of cord layers increased, the impact of the cord angle on the enhancement of vertical stiffness became more pronounced. The minimum vertical stiffness of 31.532 N/mm occurred

ISSN PRINT 1392-8716, ISSN ONLINE 2538-8460

when the number of cord layers was 2 and the cord angle was 15°, while the maximum vertical stiffness of 105.375 N/mm occurred when the number of cord layers was 6 and the cord angle was 5°.

According to Table 2 and Fig. 5(c), when the number of cord layers was constant, the vertical stiffness of the membrane air spring increased with the enlargement of the cord cross-sectional area, exhibiting a positive correlation. When the number of cord layers was 2, 4, and 6, the increases in vertical stiffness as the cord cross-sectional area rose from 0.100 to 0.283 mm^2 were 19.917 N/mm, 30.976 N/mm, and 28.468 N/mm, corresponding to growth ratios of 63.3 %, 42.6 %, and 29.7 %, respectively. These results indicate that as the number of cord layers increased, the influence of enlarging the cord cross-sectional area on the growth ratio of vertical stiffness weakened gradually.

When the cord cross-sectional area was constant, vertical stiffness increased with the number of cord layers. For cross-sectional areas of 0.100, 0.166, and 0.283 mm^2, as the number of cord layers increased from 2 to 6, the vertical stiffness increased by 64.499 N/mm, 68.500 N/mm, and 73.050 N/mm, corresponding to increase ratios of 204.9 %, 164.0 %, and 142.1 %, respectively. This indicates that, as the number of cord layers increased from 2 to 6, a larger cord cross-sectional area enhanced the overall vertical stiffness but gradually reduced its effect on the growth rate of stiffness. The minimum vertical stiffness of 31.476 N/mm occurred when the number of cord layers was 2 and the cord cross-sectional area was 0.100 mm^2, while the maximum vertical stiffness of 124.443 N/mm occurred when the number of cord layers was 6 and the cross-sectional area was 0.283 mm^2.

5. Influence of cord parameter combination on the vertical stiffness of the membrane air spring

5.1. Determination of the orthogonal experimental table

To investigate the combined effects of four factors – cord spacing, cord angle, cord cross-sectional area, and the number of cord layers – on the vertical stiffness of membrane air springs, the orthogonal experimental method was adopted [14]. The four influencing factors were the number of cord layers (t), the cord spacing (m), the cord angle (α), and the cord cross-sectional area (s). Each factor was assigned at three different levels, and the specific factors and levels are shown in Table 3.

Table 3. 4 factor 3 level numerical table

Factor level	t (layer)	m (mm)	α (°)	s (mm^2)
1	$t_1 = 2$	$m_1 = 3$	$\alpha_1 = 5$	$s_1 = 0.100$
2	$t_2 = 4$	$m_2 = 5$	$\alpha_2 = 10$	$s_2 = 0.166$
3	$t_3 = 6$	$m_3 = 7$	$\alpha_3 = 15$	$s_3 = 0.283$

Based on Table 3, an orthogonal table L_9 (3^4) was established and nine experiments were combined. The vertical stiffness of each configuration was calculated using the same method described in Section 4. The orthogonal experimental results are summarized in Table 4.

5.2. Orthogonal experimental range analysis

Range analysis, commonly represented by R, is a statistical method used to evaluate the relative influence of different factors. A larger R value indicates a greater impact of the factor on the output variable. The average values of the nine experimental groups for each factor and level are denoted as $\overline{K_{ij}}$, where i represents the level ($i = 1, 2, 3$) and j represents the factor ($j = t, m, \alpha, s$). The range R is calculated as the difference between the maximum and minimum values of $\overline{K_{ij}}$ for each factor, as shown in Eq. (11):

$$R = \max\left(\overline{K_{ij}}\right) - \min\left(\overline{K_{ij}}\right). \quad (11)$$

Using the vertical stiffness values from Table 4 and Eq. (11), the range analysis results were obtained and are presented in Table 5. Based on the calculated $\overline{K_{ij}}$ values, the influence trends of the four cord parameters at three levels were plotted, as shown in Fig. 6.

Table 4. Calculation results of 4 factors 3 levels orthogonal experiments

Group number	t (layer)	m (mm)	α (°)	s (mm^2)	K_1 (N·mm^{-1})
1	1	1	1	1	47.575
2	1	2	2	2	40.751
3	1	3	3	3	35.525
4	2	1	2	3	111.925
5	2	2	3	1	56.953
6	2	3	1	2	73.925
7	3	1	3	2	110.275
8	3	2	1	3	124.072
9	3	3	2	1	76.725

Table 5. Range analysis table

Index	t (layer)	m (mm)	α (°)	s (mm^2)
$\overline{K_1}$	41.283	89.925	81.857	60.418
$\overline{K_2}$	80.934	73.925	76.467	74.983
$\overline{K_3}$	103.691	62.058	67.584	90.507
R	62.408	27.867	14.273	30.089

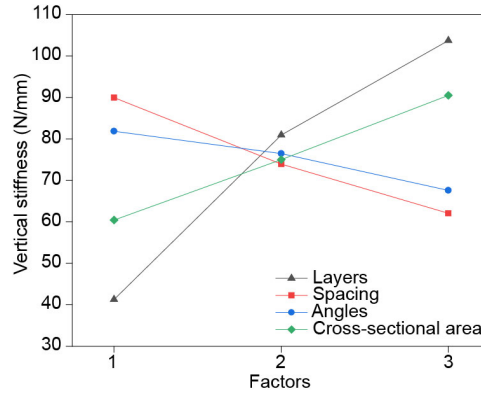


Fig. 6. Influence of four cord factors at three levels on vertical stiffness

As illustrated in Fig. 6, vertical stiffness increased significantly with the number of cord layers, indicating a strong positive correlation. As the cord cross-sectional area increased, vertical stiffness also increased, showing a relatively strong influence. Conversely, as cord spacing increased, vertical stiffness decreased, demonstrating a moderate negative effect. The influence of cord angle on vertical stiffness was the weakest, with only a minor decreasing trend observed.

According to Table 5 and Fig. 6, the order of factor influence based on the range R was: $R_t > R_s > R_m > R_\alpha$. Using maximum vertical stiffness as the evaluation criterion, the maximum $\overline{K_{ij}}$ value in each factor was selected to combine the optimal level group $t_3 m_1 \alpha_1 s_3$.

5.3. Comparative analysis of the optimal level combination

After reviewing relevant literature, the intermediate level combination $t_2 m_2 \alpha_2 s_2$ was selected as a reference for comparison with the optimal level combination $t_3 m_1 \alpha_1 s_3$, as shown in Table 3. The load-displacement curves of both configurations were obtained, as illustrated in Fig. 7.

ISSN PRINT 1392-8716, ISSN ONLINE 2538-8460

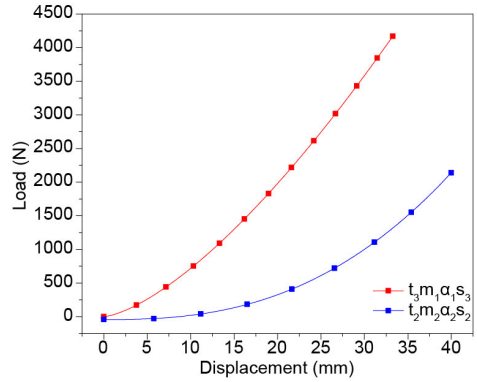


Fig. 7. Load-displacement curves of $t_3m_1\alpha_1s_3$ and $t_2m_2\alpha_2s_2$

As shown in Fig. 7, the overall load of both $t_3m_1\alpha_1s_3$ and $t_2m_2\alpha_2s_2$ combinations increased nonlinearly with displacement and the growth rate became progressively larger. At the same displacement, the load corresponding to $t_3m_1\alpha_1s_3$ was consistently higher than that of $t_2m_2\alpha_2s_2$. Furthermore, the difference in load between the two groups widened as the displacement increased. The maximum compression displacement for $t_3m_1\alpha_1s_3$ was 33.275 mm, with a corresponding load of 4169.438 N. A quartic polynomial fitting was applied to the optimal level group $t_3m_1\alpha_1s_3$ to obtain the functional relationship describing the variation law of vertical stiffness, as expressed in Eq. (12):

$$f(x) = 8.104x^4 - 26.07x^3 + 166.3x^2 + 1244x + 1420. \quad (12)$$

6. Influence of membrane air spring cord parameters on 50 mm compression displacement

To further examine the variation characteristics of vertical stiffness under a finite and larger compression displacement, the compression displacement was increased to 50 mm. Based on the four cord parameters in Table 1 – namely, the number of cord layers, cord spacing, cord angle, and cord cross-sectional area – each parameter was divided into three groups, resulting in 81 experimental combinations. The corresponding vertical stiffness values were calculated for all groups, and the results are summarized in Table 6.

In Table 6, among the groups numbered 5, 6, and 9, the results of the four parameter combinations failed to converge. In these cases, the compression displacement z and the vertical stiffness K_1 are represented by X. There were 18 groups (numbers 19, 20, 22, 46, 47, 48, 49, 50, 64, 65, 66, 73, 74, 75, 76, 77, 78, and 79) that did not reach the full compression displacement of 50 mm.

From Table 6, when the number of cord layers t was 2, 4, and 6, and the cord spacing m and angle α were 3 mm and 5°, respectively, with a cord cross-sectional area s of 0.100 mm^2, the corresponding test groups were 1, 10, and 19. When s was 0.166 mm^2, groups 28, 37, and 46 were selected. When s was 0.283 mm^2, groups 55, 64, and 73 were selected. The compression displacement z and vertical stiffness K_1 for these nine groups were compared, as illustrated in Fig. 8.

As shown in Fig. 8, the horizontal axis represents the experimental group numbers, while the vertical axis corresponds to compression displacement z and vertical stiffness K_1. When the cord spacing and angle were constant and the cord cross-sectional area values were 0.100, 0.166, and 0.283 mm^2, an increase in the number of cord layers led to a rise in vertical stiffness K_1, reaching its maximum at six layers. However, as the number of cord layers increased, the allowable compression displacement z of the membrane air spring gradually decreased, indicating a trade-off between stiffness and deformability.

Table 6. The vertical stiffness values of 81 experimental groups

Sequence number	t-m-α-s	z (mm)	K_1 (N·mm^{-1})
1	2-3-5-0.100	50.000	52.339
2	2-3-10-0.100	50.000	45.186
3	2-3-15-0.100	50.000	36.072
4	2-5-5-0.100	50.000	36.386
5	2-5-10-0.100	X	X
6	2-5-15-0.100	X	X
7	2-7-5-0.100	50.000	25.738
8	2-7-10-0.100	50.000	22.299
9	2-7-15-0.100	X	X
10	4-3-5-0.100	50.000	90.112
11	4-3-10-0.100	50.000	86.929
12	4-3-15-0.100	50.000	80.858
13	4-5-5-0.100	50.000	74.186
14	4-5-10-0.100	50.000	70.788
15	4-5-15-0.100	50.000	65.000
16	4-7-5-0.100	50.000	63.344
17	4-7-10-0.100	50.000	60.053
18	4-7-15-0.100	50.000	54.643
19	6-3-5-0.100	47.095	109.490
20	6-3-10-0.100	49.887	109.593
21	6-3-15-0.100	50.000	105.053
22	6-5-5-0.100	47.823	98.482
23	6-5-10-0.100	50.000	93.913
24	6-5-15-0.100	50.000	89.055
25	6-7-5-0.100	50.000	85.567
26	6-7-10-0.100	50.000	83.176
27	6-7-15-0.100	50.000	78.304
28	2-3-5-0.166	50.000	67.310
29	2-3-10-0.166	50.000	57.758
30	2-3-15-0.166	50.000	45.719
31	2-5-5-0.166	50.000	52.198
32	2-5-10-0.166	50.000	45.067
33	2-5-15-0.166	50.000	35.979
34	2-7-5-0.166	50.000	41.761
35	2-7-10-0.166	50.000	36.159
36	2-7-15-0.166	50.000	28.960
37	4-3-5-0.166	50.000	105.015
38	4-3-10-0.166	50.000	101.738
39	4-3-15-0.166	50.000	96.672
40	4-5-5-0.166	50.000	89.972
41	4-5-10-0.166	50.000	86.784
42	4-5-15-0.166	50.000	80.714
43	4-7-5-0.166	50.000	79.553
44	4-7-10-0.166	50.000	76.169
45	4-7-15-0.166	50.000	70.248
46	6-3-5-0.166	40.058	118.181
47	6-3-10-0.166	41.846	118.659
48	6-3-15-0.166	48.329	118.834
49	6-5-5-0.166	46.877	109.268
50	6-5-10-0.166	47.469	108.169
51	6-5-15-0.166	50.000	104.913
52	6-7-5-0.166	50.000	100.935
53	6-7-10-0.166	50.000	99.231
54	6-7-15-0.166	50.000	94.428

Sequence number	t-m-α-s	z (mm)	K_1 (N·mm^{-1})
55	2-3-5-0.283	50.000	82.250
56	2-3-10-0.283	50.000	69.867
57	2-3-15-0.283	50.000	54.682
58	2-5-5-0.283	50.000	67.947
59	2-5-10-0.283	50.000	58.285
60	2-5-15-0.283	50.000	46.116
61	2-7-5-0.283	50.000	58.116
62	2-7-10-0.283	50.000	50.077
63	2-7-15-0.283	50.000	39.861
64	4-3-5-0.283	43.248	116.212
65	4-3-10-0.283	43.417	114.649
66	4-3-15-0.283	49.258	107.954
67	4-5-5-0.283	50.000	105.570
68	4-5-10-0.283	50.000	103.314
69	4-5-15-0.283	50.000	97.362
70	4-7-5-0.283	50.000	95.886
71	4-7-10-0.283	50.000	92.942
72	4-7-15-0.283	50.000	86.858
73	6-3-5-0.283	33.300	124.062
74	6-3-10-0.283	35.692	126.471
75	6-3-15-0.283	43.183	128.421
76	6-5-5-0.283	41.634	124.072
77	6-5-10-0.283	43.183	120.357
78	6-5-15-0.283	46.972	118.314
79	6-7-5-0.283	44.068	113.057
80	6-7-10-0.283	50.000	115.241
81	6-7-15-0.283	50.000	110.893

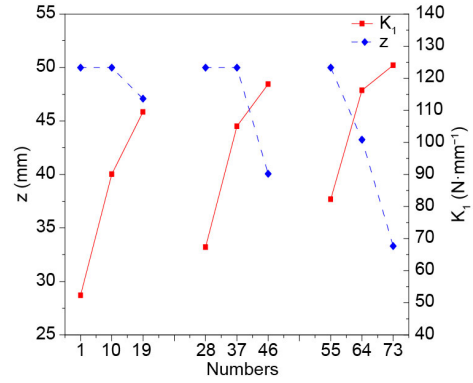


Fig. 8. Influence of the number of cord layers on compression displacement z and vertical stiffness K_1 of the membrane air spring

According to Table 6, when the cord spacing (m) was 3, 5, and 7 mm, and the number of cord layers t and angle α were fixed at six layers and 5°, respectively, while the cord cross-sectional area s was 0.100 mm^2, the selected groups were 19, 22, and 25. When s was 0.166 mm^2, groups 46, 49, and 52 were selected, and when s was 0.283 mm^2, groups 73, 76, and 79 were selected. The compression displacement z and vertical stiffness K_1 for these nine groups were compared, as shown in Fig. 9.

As is illustrated in Fig. 9, the horizontal axis represents the group numbers, and the vertical axis indicates the compression displacement z and vertical stiffness K_1, respectively. When the number of cord layers and the cord angle were constant, and the cord cross-sectional areas were 0.100, 0.166, and 0.283 mm^2, and the compression displacement z that the membrane air spring

could withstand decreased progressively with increasing cord spacing. Meanwhile, vertical stiffness K_1 also decreased as cord spacing increased, exhibiting a clear negative correlation between cord spacing and vertical stiffness.

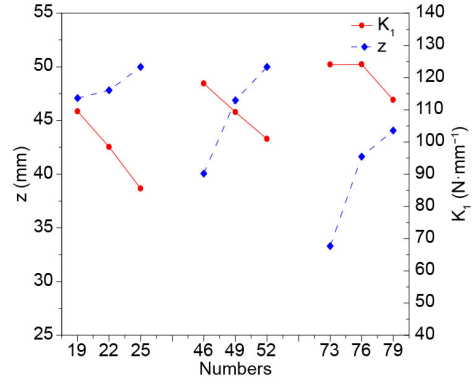


Fig. 9. Influence of cord spacing on compression displacement z and vertical stiffness K_1 of the membrane air spring

According to Table 6, when the cord cross-sectional areas (s) were 0.100, 0.166, and 0.283 mm^2, and the number of cord layers (t) and the cord angle (α) were fixed at six layers and 5°, respectively, with cord spacing (m) set to 3 mm, groups 19, 46, and 73 were selected. When m was 5 mm, groups 22, 49, and 76 were used; when m was 7 mm, groups 25, 52, and 79 were selected. The compression displacement z and vertical stiffness K_1 for these nine groups were compared, as illustrated in Fig. 10.

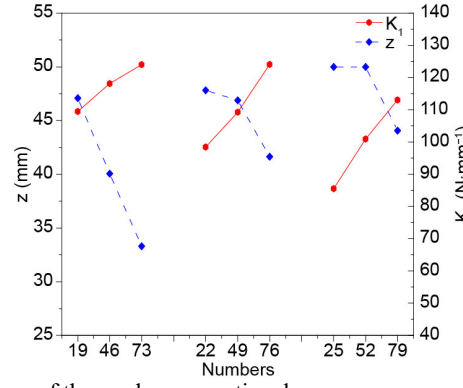


Fig. 10. Influence of the cord cross-sectional area on compression displacement and vertical stiffness of the membrane air spring

As shown in Fig. 10, the horizontal axis represents the experimental group number, while the vertical axis denotes the compression displacement z and vertical stiffness K_1. When the number of cord layers and cord angle were constant, and the cord spacing values were 3, 5, and 7 mm, the compression displacement z that the membrane air spring could withstand gradually decreased with an increase in the cord cross-sectional area. Meanwhile, vertical stiffness K_1 increased progressively with increasing cross-sectional area, demonstrating a positive correlation between the two.

According to Table 6, when the cord angle (α) was 5°, 10°, and 15°, and the number of cord layers (t) and cord spacing (m) were fixed at six layers and 3 mm, respectively, with the cord cross-sectional area (s) set to 0.100 mm^2, groups 19, 20, and 21 were selected. When s was 0.166 mm^2, groups 46, 47, and 48 were used, and when s was 0.283 mm^2, groups 73, 74, and 75

ISSN PRINT 1392-8716, ISSN ONLINE 2538-8460

were taken. The compression displacement z and vertical stiffness K_1 of these nine groups were compared, as shown in Fig. 11.

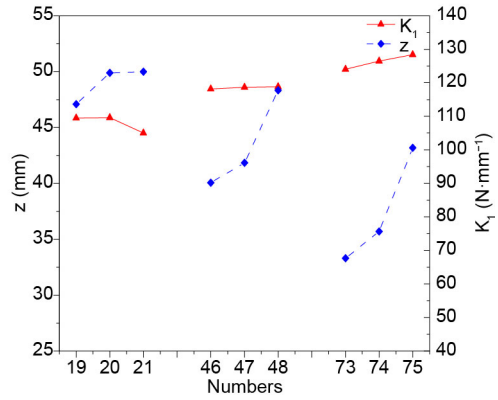


Fig. 11. Influence of cord angle on compression displacement and vertical stiffness of the membrane air spring

As illustrated in Fig. 11, the horizontal axis represents the experimental group numbers, and the vertical axis represents compression displacement z and vertical stiffness K_1. When the number of cord layers and cord spacing remained unchanged, and the cord cross-sectional areas were 0.100, 0.166, and 0.283 mm^2, the compression displacement z that the membrane air spring could withstand increased gradually with the increase in cord angle. For groups 19, 20, and 21, vertical stiffness K_1 showed a decreasing trend with increasing cord angle, while for groups 46, 47, 48 and groups 73, 74, 75, vertical stiffness K_1 exhibited an increasing trend. These results indicate that the effect of cord angle on vertical stiffness is non-monotonic and may depend on the combination of other cord parameters.

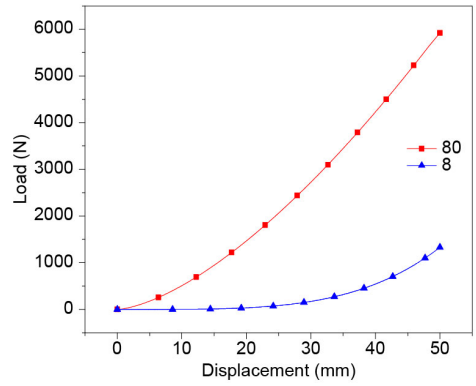


Fig. 12. Load-displacement curves of Group 8 and Group 80

Based on the data in Table 6, among all experimental groups that achieved a compression displacement of 50 mm, the combination of four cord parameters resulting in the smallest vertical stiffness corresponded to group 8, while the combination producing the largest vertical stiffness corresponded to group 80. The load-displacement curves for groups 8 and 80 were plotted and are presented in Fig. 12.

As shown in Fig. 12, the loads sustained by both groups increased with increasing displacement. Under the same compression displacement, the six-layer cord configuration withstood a higher load than the two-layer cord configuration. Furthermore, at each displacement level, the load value of group 80 was greater than that of group 8, and the difference in load

between the two groups widened progressively as displacement increased.

7. Conclusions

To investigate the vertical stiffness characteristics of membrane air springs within a confined installation space, the influence of rubber airbag cord parameters on vertical stiffness was analyzed. A three-dimensional model of the membrane air spring was developed using SolidWorks, and its vertical stiffness behavior was simulated through ABAQUS. The effects of four key cord parameters – number of cord layers, cord spacing, cord angle, and cord cross-sectional area – on the vertical stiffness were systematically examined. The main conclusions are summarized as follows:

1) The influence characteristics of the four cord parameters on the vertical stiffness of membrane air springs were analyzed individually. When three parameters remained constant and only one was varied, the vertical stiffness of the membrane air spring decreased with increasing cord spacing and cord angle, while it increased with larger cord cross-sectional area and greater number of cord layers.

2) Based on the orthogonal experimental design method, the relative importance of the four cord parameters influencing vertical stiffness was determined. The number of cord layers exhibited the most significant effect on vertical stiffness, with an increase in layer count producing a pronounced enhancement in stiffness. The effects of cord spacing and cord cross-sectional area were moderate in comparison, while the cord angle had the least influence.

3) When the compression displacement was set to 50 mm, the combined influence of the four cord parameters on vertical stiffness was analyzed, and the parameter combinations yielding the minimum and maximum stiffness values were identified. The minimum vertical stiffness occurred when the number of cord layers was 2, the cord spacing was 7 mm, the cord angle was 10°, and the cord cross-sectional area was 0.100 mm^2. The maximum vertical stiffness was obtained when the number of cord layers was 6, the cord spacing was 3 mm, the cord angle was 15°, and the cord cross-sectional area was 0.283 mm^2.

The above research findings offer theoretical support for subsequent bench testing. Moving forward, bench tests targeting the membrane air spring will be carried out systematically. Drawing on the ensuing test data and analytical, it will provide references for the structural optimization and performance enhancement of membrane air spring.

Acknowledgements

This work was supported by Research Foundation of Shaanxi University of Technology under Grant SLGRCQD2321 and Shaanxi Province Key Research and Development Foundation under Grant 2025CY-JJQ-20.

Data availability

The datasets generated during and/or analyzed during the current study are available from the corresponding author on reasonable request.

Author contributions

Xufei Wang: funding acquisition, methodology, review and editing, original draft preparation. Zhiqiang Xie: conceptualization, data curation, original draft preparation, visualization. Ningchao Zhang: software, data validation. Jinde Song: funding acquisition, resources.

Conflict of interest

The authors declare that they have no conflict of interest.

References

[1] C. Yuan, K. Zhou, G. Wang, D. An, and L. Wu, "Simulation and experimental investigation of mechanical property of air spring for vehicles," (in Chinese), *Transactions of the Chinese Society of Agricultural Engineering*, Vol. 24, No. 3, pp. 38–42, Jan. 2008, https://doi.org/10.3321/j.issn:1002-6819.2008.03.008

[2] W. Zhou, C. Zhang, Y. Zhang, and Q. Li, "Simulation analysis on vertical stiffness characteristics of air spring for a tractor," (in Chinese), *Machinery Design and Manufacture*, No. 8, pp. 170–173, Jan. 2018, https://doi.org/10.3969/j.issn.1001-3997.2018.08.049

[3] H. Lee and C.-S. Kim, "Prediction of ply angles of air springs according to airbag positions and their effects on lateral and torsional stiffness," *Applied Sciences*, Vol. 12, No. 22, p. 11815, Nov. 2022, https://doi.org/10.3390/app122211815

[4] D. Zhang, Q. Liu, J. Xie, H. Zuo, and Q. Wang, "Effect of cord parameters on vertical stiffness of rubber air spring," (in Chinese), *Journal of Machine Design*, Vol. 40, No. 11, pp. 62–68, Nov. 2023.

[5] Z. Lu, P. Si, H. Xiao, and J. Liu, "Influence of aging time on vertical static stiffness of air spring," *Applied Sciences*, Vol. 12, No. 9, p. 4219, Apr. 2022, https://doi.org/10.3390/app12094219

[6] L. Yin, W. Xu, Z. Hu, M. He, and C. Li, "Research on damping and vibration absorption performance of air spring dynamic vibration absorber," *Journal of Vibration Engineering and Technologies*, Vol. 12, No. 3, pp. 3771–3782, Jul. 2023, https://doi.org/10.1007/s42417-023-01083-4

[7] S. Oman and M. Nagode, "The influence of piston shape on air-spring fatigue life," *Fatigue and Fracture of Engineering Materials and Structures*, Vol. 41, No. 5, pp. 1019–1031, Nov. 2017, https://doi.org/10.1111/ffe.12748

[8] G. Marini et al., "On optimal control of a multichamber air spring and experimental validation over speed bumps," *IFAC-PapersOnLine*, Vol. 56, No. 2, pp. 1989–1994, Jan. 2023, https://doi.org/10.1016/j.ifacol.2023.10.1093

[9] Y. Hu, J. Zhang, and J. Long, "Influence of rubber's viscoelasticity and damping on vertical dynamic stiffness of air spring," *Scientific Reports*, Vol. 13, No. 1, p. 9886, Jun. 2023, https://doi.org/10.1038/s41598-023-36904-9

[10] K. Arai, H. Akimichi, and M. Hirata, "Precise measurements of the volume change in a bellows by Boyle's law," in *SICE Annual Conference 2005, Okayama, Japan*, pp. 119–122, 2005.

[11] M. Zhu, *Engineering thermodynamics*. Beijing: Tsinghua University Press, 1995.

[12] M. Wu et al., "A theoretical model of amplitude-dependent dynamical stiffness for cord-rubber air springs," *Proceedings of the Institution of Mechanical Engineers, Part L: Journal of Materials: Design and Applications*, Vol. 237, No. 2, pp. 425–436, Aug. 2022, https://doi.org/10.1177/14644207221117270

[13] K. Chunyan, X. Jie, Y. Mingkun, L. Yang, and L. Yi, "Analysis of static and dynamic characteristics of membrane air springs for small passenger cars," *Journal of the Brazilian Society of Mechanical Sciences and Engineering*, Vol. 46, No. 12, p. 682, Nov. 2024, https://doi.org/10.1007/s40430-024-05244-8

[14] J. Seberry, *Orthogonal Designs: Hadamard Matrices, Quadratic Forms and Algebras*. Cham, Switzerland: Springer, 2017.



Xufei Wang received the B.S. degree in mechanical engineering from Shaanxi University of Technology, China, in 1999, and received the M.S. degree in mechanical engineering from Xinjiang University, China, in 2007, and received the Ph.D. degree in computer engineering from Pai Chai University, South Korea, in 2022. Now he works as a professor at Shaanxi University of Technology in China. His research interest includes system modeling and simulating, control and dynamics.



Zhiqiang Xie is currently pursuing a Master's degree in mechanical engineering at Shaanxi University of Technology, China. His research interests include vibration testing and automotive active suspension.



Ningchao Zhang is currently pursuing a Master's degree in mechanical engineering at Shaanxi University of Technology, China. His research interests include the manufacturing processes of vehicle vibration components.



Jinde Song received the B.S. degree in information and electronics in 1993. He is a senior engineer at the level of researcher in mechanical engineering and a master's supervisor. Now he works at Jiangsu Zhonggui Heavy Industry Co., Ltd. Yancheng, China. His research interest includes performance analysis of intelligent equipment.

ISSN PRINT 1392-8716, ISSN ONLINE 2538-8460